Pre-print version of: Ziółkowski, P., Koulali, A., Radomski, P., De Biase, D., Zaccagnini, F., Zieliński, J., Pikuła, M., Jeong, K.- un, Petronella, F., De Sio, L., & Mikielewicz, D. (2024). BACTERIAL INACTIVATION VIA LASER-DRIVEN GOLD NANOPARTICLE HEATING: SIMULATION AND ANALYSIS. https://doi.org/10.1615/tfec2024.bio.051260

ASTFE
American Society of Thermal and Fluids Engineers

9th Thermal and Fluids Engineering Conference (TFEC)
April, 21-24, 2024
Partially Online Virtual and at Oregon State University, OR

TFEC-2024-xxxxx

BACTERIAL INACTIVATION VIA LASER-DRIVEN GOLD NANOPARTICLE HEATING: SIMULATION AND ANALYSIS

P. Ziółkowski,[1,*] A. Koulali,[1] P. Radomski,[1] D. De Biase,[2] F. Zaccagnini,[2] J. Zieliński,[3] M. Pikuła,[3] K. Jeong,[4] F. Petronella,[5] L. De Sio,[2] D. Mikielewicz[1]

[1]Gdańsk University of Technology, Faculty of Mechanical Engineering and Ship Technology, Poland
[2]Department of Medico-Surgical Sciences and Biotechnologies Sapienza University of Rome, Latina, Italy
[3]Medical University of Gdańsk, Gdańsk, Poland
[4]Department of Polymer-Nano Science and Technology, Department of Nano Convergence Engineering, Jeonbuk National University, Jeonju, Republic of Korea
[5]National Research Council of Italy, Institute of Crystallography CNR-IC, Montelibretti, Italy

ABSTRACT

This study utilizes CFD technique to simulate the inactivation of *E. coli* bacteria within a microfluidic chamber, employing gold nanoparticles irradiated by a laser beam. Employing a single-phase model, the presence of bacteria is considered by treating thermal properties in the governing equations as effective, combining those of water and bacteria using established correlations from scientific literature. The conversion of light into heat is modeled with parameters derived from scientific literature, featuring a defined source term quantifying the converted light into heat. Introducing a User Defined Scalar (UDS) employing a first-order kinetic model described by the Arrhenius equation for the decay coefficient captures the bacteria's response to irradiation. A dedicated User Defined Function (UDF) is developed to implement this model, allowing the simulation to account for the reduction in bacterial concentration over time. The results uncover intricate dynamics in bacterial response to laser-induced thermal effects, showcasing the potential for effective bacterial control. Furthermore, the model is rigorously validated against experimental data, affirming its accuracy and robustness in reproducing real-world thermal effects.

KEY WORDS: CFD, Heat transfer, Phototermoablation, First order kinetic model, Bacteria inactivation

NOMENCLATURE

A	pre-exponential factor	(-)	R_0	reflection coefficient of glass	(-)
M	number of gold nanoparticles	(-)	L_{p-hi}	interaction length of the i-particle	(m)
N	bacteria cell number	(-)	m_{Au}	refractive index of gold	(-)
σ_{abs_i}	absorption coefficient of the i-particles	(m^{-1})	m_{gl}	refractive index of glass	(-)
I_0	initial intensity of laser	(W/m^2)	K	decay coefficient	$(1/s)$
β_I	incident angle	(rad)			

*Corresponding P. Ziółkowski: pawel.ziolkowski1@pg.edu.pl

1. INTRODUCTION

1.1 Literature review

Laser-based bacteria inactivation, spanning medical sterilization [1], water treatment [2], food safety [3], and air purification [4], is pivotal in eliminating bacteria. This approach is crucial in dentistry for aseptic conditions, biomedical research, and pharmaceutical manufacturing sterility. Laser precision provides a chemical-free solution, advancing health, safety, and research. Expanding on laser bacteria inactivation, an intriguing application involves laser heat treatment with gold nanoparticles [5–9]. This technique utilizes laser energy to induce controlled heating in the presence of gold nanoparticles, offering precise temperature elevation. With exceptional heat absorption, gold nanoparticles find applications in targeted cancer therapy and precise drug delivery, showcasing the potential for controlled heat in medical and scientific interventions.

In the exploration of laser heat treatment of gold nanoparticles, research efforts adopt mainly experimental procedures [10–12] . While experimentation provides concrete results, it should be noted that theoretical or simulation approaches remain relatively rare in this field. Our own research addresses this area, using computational fluid dynamics (CFD) techniques to study the inactivation of bacteria in a microfluidic chamber using laser-irradiated gold nanoparticles. The distinctive advantage of CFD lies in its ability to provide insight into complex fluid dynamics and heat transfer processes, enabling a comprehensive understanding of the phenomena. This method is particularly useful for predicting complex reaction of bacteria to temperature rise, enabling experimental set-ups to be optimized. However, it is essential to recognize limitations, such as the need for accurate model validation and potential simplifications that can influence real-world accuracy. Despite these constraints, the integration of CFD with experimental approaches holds promise for improving our understanding of laser treatments with gold nanoparticles or other phenomena based on micro and nanoscale [13].

When CFD techniques are employed to study bacterial deactivation mechanisms, a key problem is how to describe this phenomenon accurately. Several papers have taken up this challenge, initially using kinetic models. This approach provides a quantitative representation of the deactivation process, offering insight into the speed and efficiency of bacterial inactivation in the system under study. By adopting kinetic order models, researchers seek to explain the complex dynamics of bacterial deactivation, laying the foundations for a comprehensive understanding of the processes involved. Research exploiting CFD techniques for bacterial inactivation includes studies on the thermal treatment of water for potabilization purposes (see [14, 15]). In the work carried out by [14], researchers have used 3D CFD models and kinetic simulations to analyse chlorine decay, pathogen inactivation, and by-product formation in disinfection contact tanks. Unlike traditional approaches reliant on Hydraulic Efficiency Indicators, the study optimizes hydrodynamics, showing that improved conditions lead to uniform disinfectant contact times, enhancing pathogen inactivation and controlling by-product accumulation in various CT design variations.

In the work carried out on UV-LED water disinfection validation using a numerical CFD model [16], the authors conducted hydraulic analysis, characterized light distribution, and performed microbial dose–response testing. Their research showcases agreement between simulations and experiments, providing crucial insights for designing UV LED reactors in point-of-use water disinfection, particularly in developing countries. Beyond the mentioned applications, CFD has been extensively applied in exploring thermal inactivation of bacteria in various contexts. Within the realm of medical devices, CFD simulations have been employed to optimize the design of heat-based disinfection systems for surgical instruments ([17–19]), ensuring the elimination of bacteria and ensuring aseptic conditions. The researchers in [19] developed a computational fluid dynamics (CFD) model, incorporating bacterial spore inactivation kinetics and validating it with measurements. They derived these kinetics from experimental data involving wet steam, water and two dialysis solutions. The simulations, focusing on sterilization efficiency and the distribution of non-condensable gases, demonstrate the model's versatility. This CFD model, with its underlying equations representing inactivation kinetics, provides a solid framework for researchers to advance sterilization processes and ensure enhanced product safety.

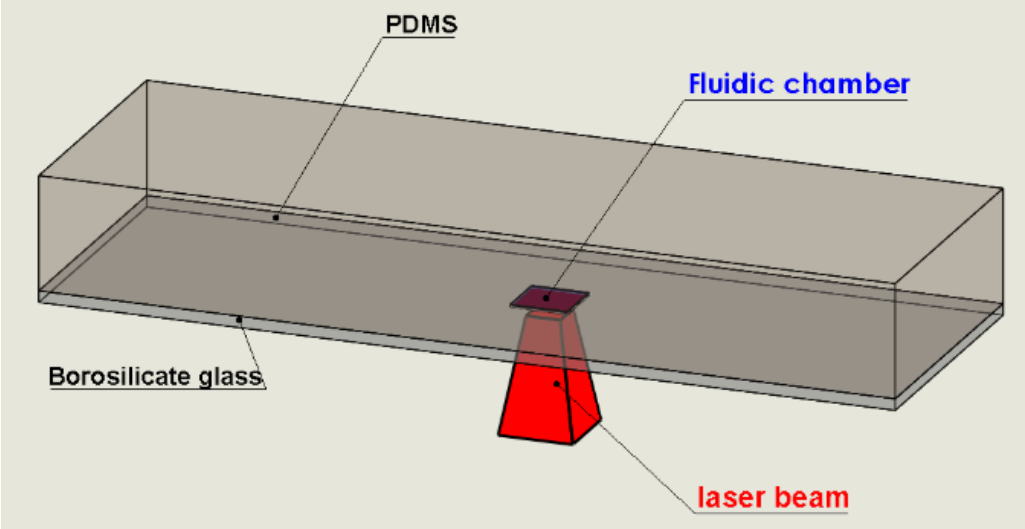

Fig. 1 Physical model

In environmental engineering, CFD plays a crucial role in modeling and analyzing the thermal inactivation of bacteria in wastewater treatment plants, guiding the development of efficient and sustainable sanitation processes ([20, 21]). In addition to these applications, CFD's versatility in thermal bacteria inactivation spans HVAC systems, biofuel production, and industrial processes. All the above-mentioned works employing CFD for thermal inactivation of bacteria rely on first-order kinetic equations, encapsulated as $N(t) = N_0 \cdot e^{-k \cdot t}$. This mathematical formulation integrates to establish a comprehensive model for bacterial inactivation (see [22–24]). The calculation of the inactivation rate (k) follows the widely applied Arrhenius equation: $k = A \cdot e^{-\frac{\Delta E}{RT}}$. This technique, grounded in the dynamic interplay between temperature and inactivation kinetics, offers a nuanced understanding of the thermal processes governing bacterial deactivation in CFD-based studies.

1.2 Motivation and novelty

In view of the increasing global threat of antibiotic resistance, innovative approaches to combating bacteria must be explored. Bacteria inactivation by laser, coupled with gold nanoparticles, offers the promise of revolutionizing microbiology, healthcare and biotechnology. However, there is a major gap in the literature - the limited application of computational fluid dynamics (CFD) methods in this context. This gap becomes even more important when we consider the urgent need for more sustainable and effective bacterial control strategies. Our research integrates laser technology and gold nanoparticles for bacterial control, and introduces a novel aspect by using CFD methods. Most studies in this field rely heavily on experimental procedures, leaving the potential of CFD techniques largely unexplored. Numerical simulation analysis in a microfluidic chamber, incorporating gold nanoparticles, offers a unique perspective of the thermal effects on bacterial inactivation. This approach, distinct from traditional experimental methodologies, helps to bridge the existing gap, offering the possibility of examining a wide range of control parameters.

2. GERMICIDAL MICROCHAMBER DEVICE

Our germicidal microchamber device, designed for the thermal inactivation of *E. coli* bacteria, comprises a slender chamber with a surface area of $5 \times 5\,\mathrm{mm}^2$ and a height (h) of 10 micrometers. The construction involves securing a 1 mm-thick borosilicate glass plate and insulating it with a 1 cm-thick layer of PDMS organic glass. The chamber's dimensions are illustrated in Figure 1. Gold nanoparticles (AuNPs) are incorporated into the chamber's bottom, treated as a thin film with a thickness ($L_{\text{p-hi}}$) of 23 nm. The device is exposed to a laser beam. Notably, only a $3 \times 3\,\mathrm{mm}^2$ area of the gold nanoparticle slab was irradiated.

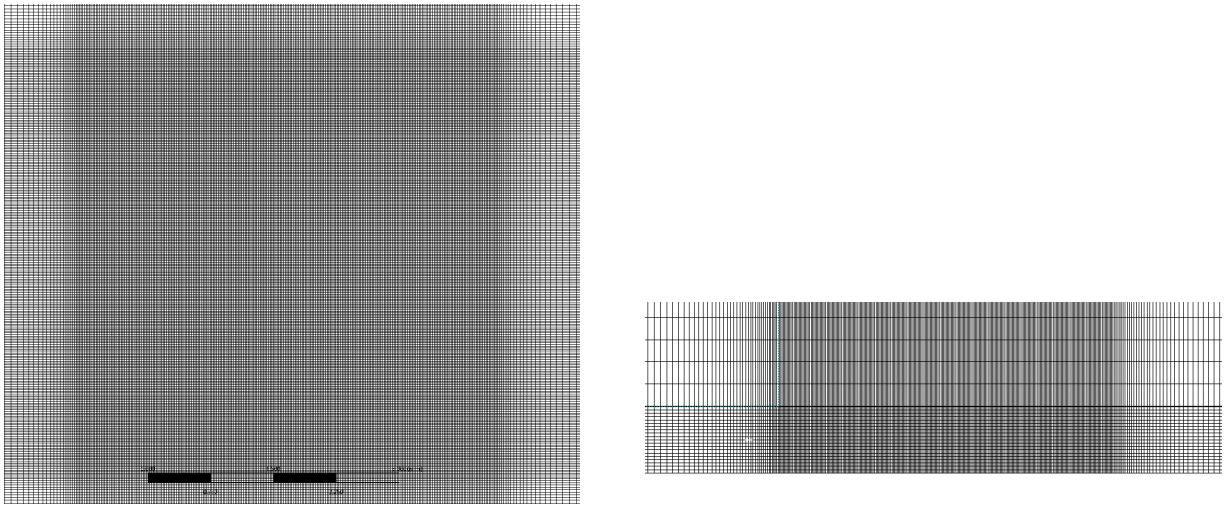

Fig. 2 Mesh grid generation

Table 1 Mesh characteristics

	Fluidic chamber			The whole system	
	Node number	Element number	Maximum aspect ratio	Node number	Element number
M1	91809	80000	40	364361	3480000
M2	296413	270000	40	5668465	542500
M3	727218	680000	42.5	8382370	8040000
M4	1323021	1250000	40	8382370	8040000
M5	2160000	2160000	40	15387877	14800000

3. MATHEMATICAL FORMULATION AND NUMERICAL PROCEDURE

3.1 Single phase formulation

CFD equations The mass conservation, also known as the continuity equation, describes the conservation of mass of fluid flow, it can be written in the case of 3D flow in unsteady state with laminar regime as fellow:

$$\frac{\partial \rho_{\text{eff}}}{\partial t} + \nabla \cdot (\rho_{\text{eff}} \vec{v}) = 0 \tag{1}$$

Momentum equation

$$\frac{\partial (\rho_{\text{eff}} \vec{v})}{\partial t} + \nabla \cdot (\rho_{\text{eff}} \vec{v}) = -\nabla p + (\mu_{\text{eff}} [(\nabla \vec{v} + \nabla \vec{v}^{\text{tr}}) - \frac{2}{3} \nabla \cdot \vec{v} I]) + \rho_{\text{eff}} \vec{g} \tag{2}$$

Energy equation

$$\frac{\partial (\rho_{\text{eff}} cp_{\text{eff}} T_{\text{f}})}{\partial t} + \nabla \cdot (\vec{v} (\rho_{\text{eff}} cp_{\text{eff}} T_{\text{f}})) = \nabla \cdot (k_{\text{eff}} \nabla T_{\text{f}}) \tag{3}$$

Conduction equation govern the transport of scalar quantity (temperature) inside the solid region

$$\rho_{s_i} \frac{\partial (cp_{s_i} T_{s_i})}{\partial t} = \nabla \cdot (k_{s_i} \nabla T_{s_i}) \tag{4}$$

Effective thermal properties In order to take into account the presence of bacteria *E.coli* cells inside the water, the thermal properties appeared in the above-equations, can be determined using the fallowing equations

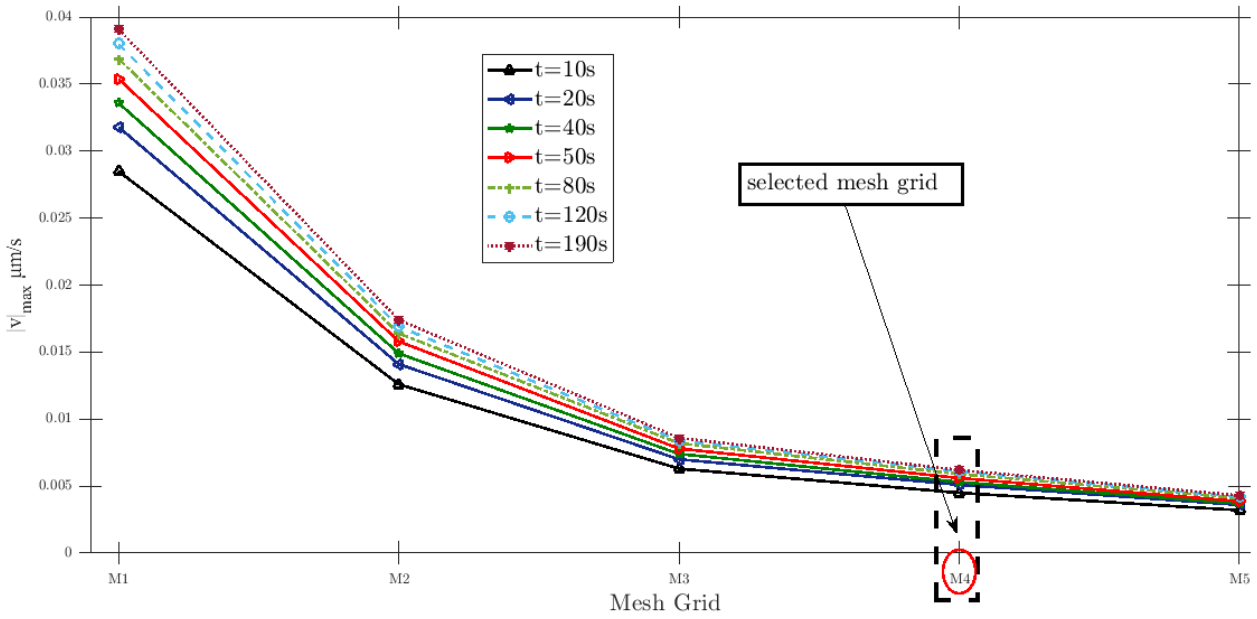

Fig. 3 Mesh grid generation

([25]):

$$\rho_{\text{eff}} = (1-\phi)\rho_{\text{w}} + \phi\rho_{\text{bac}} \tag{5}$$

$$(\rho cp)_{\text{eff}} = (1-\phi)(\rho cp)_{\text{w}} + \phi(\rho cp)_{\text{bac}} \tag{6}$$

$$(\rho\beta)_{\text{eff}} = (1-\phi)(\rho\beta)_{\text{w}} + \phi(\rho\beta)_{\text{bac}} \tag{7}$$

Effective dynamic viscosity with Brinkman model [26]:

$$\mu_{\text{eff}} = \frac{\mu_{\text{w}}}{(1-\phi)^{2.5}} \tag{8}$$

Effective thermal conductivity with Lewis and Nielsen model :

$$k_{\text{eff}} = \frac{1 + S(\frac{k_{\text{bac}}/k_{\text{w}}-1}{k_{\text{bac}}/k_{\text{w}}+S})\phi}{1 - (\frac{k_{\text{bac}}/k_{\text{w}}-1}{k_{\text{bac}}/k_{\text{w}}+S})(1+(\frac{1-\phi_{\text{m}}}{\phi_{\text{m}}^2})\phi)\phi} \tag{9}$$

The thermal properties of water depend on the temperature.

3.2 Boundary conditions

Converted light to heat in the gold slab (see [9] and [27])

$$q = \sum_{i=1}^{M} \sigma_{\text{abs}_i} \cdot I_{\text{abs}_i} = \sum_{i}^{M} \left(\sigma_{\text{abs}_i} \cdot I_0 \cdot (1-R_0) \left(1 - exp\left(-\sum_{i}^{M} \sigma_{\text{abs}_i} \cdot L_{\text{p-hi}} \left(1 - sin^2\beta \cdot \left(\frac{m_{Au}^2}{m_{gl}^2} \right) \right)^{1/2} \right) \right) \right) \tag{10}$$

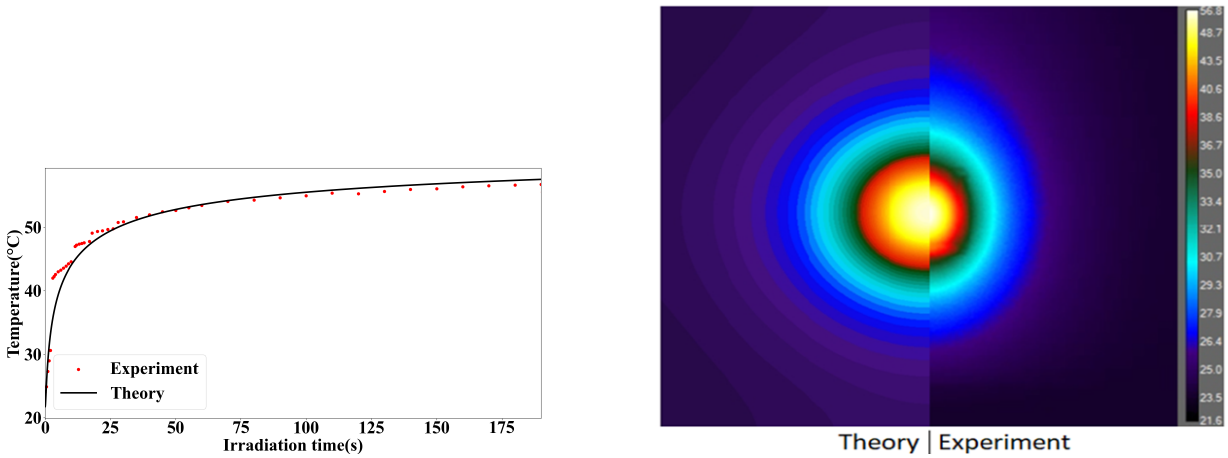

(a) (b)

Fig. 4 Validation with benchmark case : (a) maximal temperature evolution on the glass bottom vs time, (b) temperature field after $t = 190s$ on the glass bottom for P=0.8 W

The thermal boundary condition at slab gold can be expressed by:

$$q = k_{\text{gold}}(\nabla T)_{\text{gold}} = k_{\text{f}}(\nabla T)_{\text{f}}, \quad T_{\text{gold}} = T_{\text{f}} \tag{11}$$

Mixed convection/radiation condition at the glass bottom (see [28]):

$$q_{\text{tot}} = h_{\text{ext}}(T_{\infty} - T_{\text{w}}) + \epsilon\sigma(T_{\text{ext}}^4 - T_{\text{w}}^4) \tag{12}$$

Heat flux continuity at interfaces fluid/solid and solid/solid (see [28]):

$$\begin{aligned} k_{\text{f}}(\nabla T_{\text{f}}) &= k_{\text{s}_i}(\nabla T_{\text{s}_i}) \\ k_{\text{s}_i}(\nabla T_{\text{s}_i}) &= k_{\text{s}_i}(\nabla T_{\text{s}_i}) \end{aligned} \tag{13}$$

Other walls

$$\nabla T_{\text{s}} = 0 \tag{14}$$

The no slip-velocity condition was adopted at the chamber walls as fellow:

$$u, v, w = 0 \tag{15}$$

3.3 Bacteria deactivation kinetics

One commonly used model is the first-order kinetics model [22–24], as follows:

$$\frac{dN}{dt} = -KN \tag{16}$$

Where $\frac{dN}{dt}$ is the change rate of the bacteria population over time, N is the number of viable bacteria, and K is the first-order rate constant. The negative sign indicate that the population is decreasing over the time. Then, the number of bacteria survivors N is described as :

$$N = N_0 e^{-K(T)t} \tag{17}$$

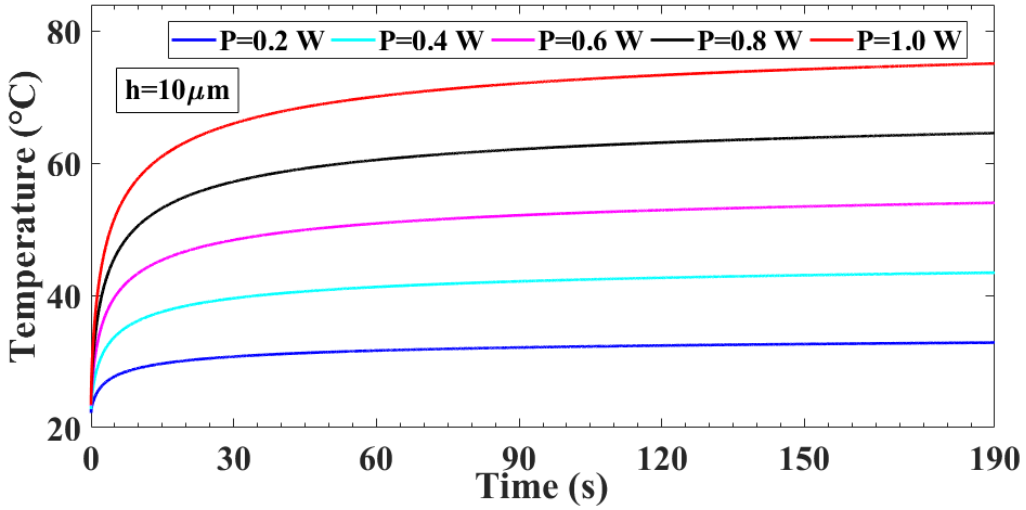

Fig. 5 Effect of power laser level on maximum temperature evolution of the mixture bacteria-water

Where N_0 is the initial number of bacterial cells and $K(T)$ is modelled with the Arrhenius equation :

$$K(T) = Ae^{-\Delta E/(RT)} \tag{18}$$

A is the pre-exponential factor, ΔE is the activation energy and R is the gas-law constant. For constant temperature at time t , the survival ratio can be expressed as: (see [22])

$$Ln(\frac{N}{N_0}) = -Ae^{-\Delta E/(RT)}t \tag{19}$$

For dynamic temperature (see [22])

$$Ln(\frac{N}{N_0}) = -\int Ae^{-\Delta E/(RT)}dt \tag{20}$$

In our case the temperature T is function of space (x, y, z) and time (t).

3.4 Numerical simulation

UDFs implementation

- UDFs for Single-Phase approach and temperature dependence: UDFs (with $define - PROPERTY$ macro) were employed to incorporate the temperature-dependent effective thermal properties of the bacteria-water mixture using equations (5 to 9) in the simulation,
- an UDS representing active microorganisms was added to the CFD model, and a source term was added to calculate microorganism inactivation using a (UDF) (With $define - source$ macro).

Fluent set-up

- ANSYS software, was utilized for geometry design and mesh generation, where a structured mesh grid was used in the simulation of the micro device to reduce the computational time. A special mesh treatment was applied at the microchamber boundaries because of the high-temperature gradient across these regions (see Figure 2). Where the bias technique was used and the bias factor was calculated in such way

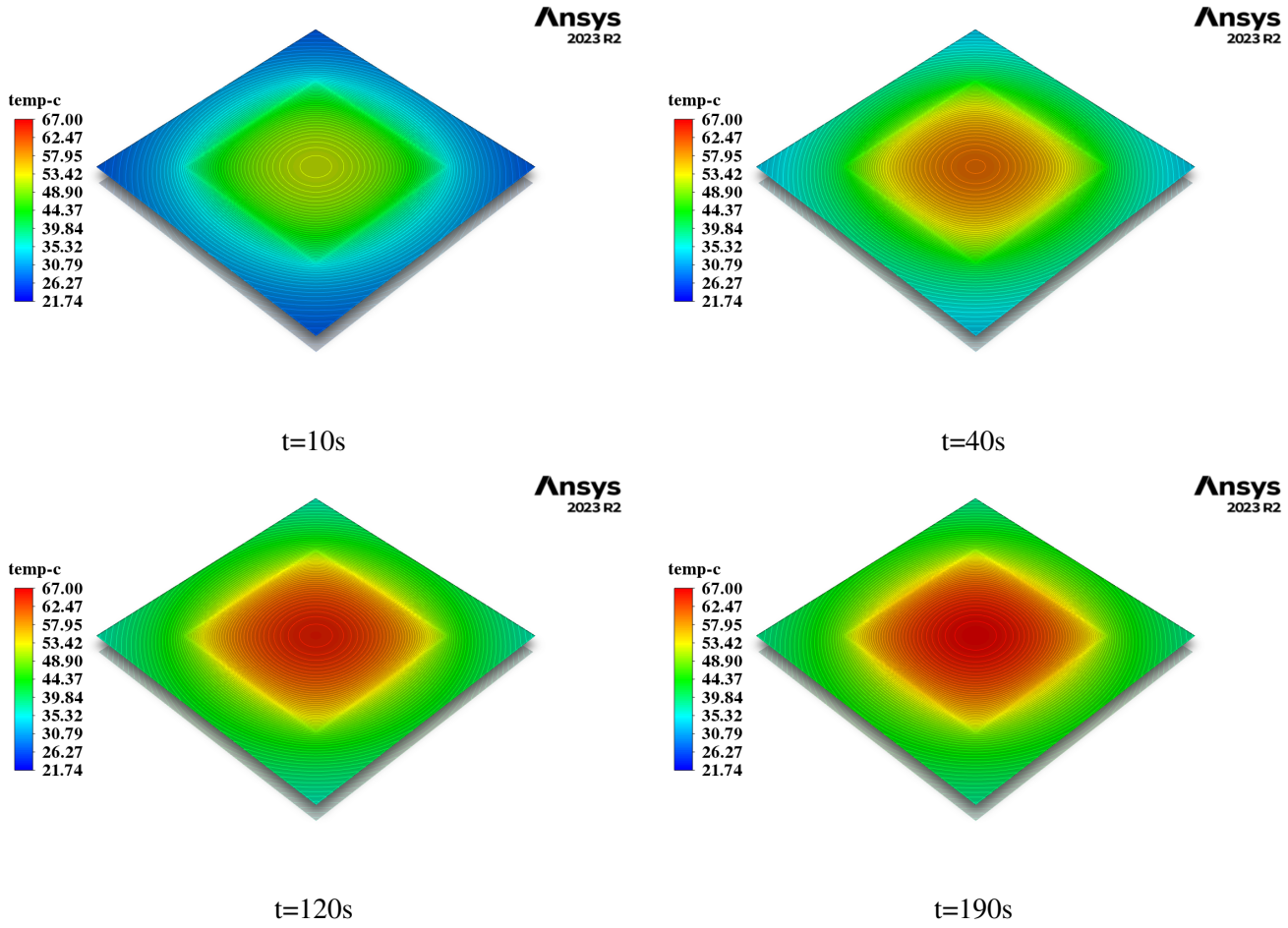

Fig. 6 Temperature field at different moment of irradiation, for P=0.8 W corresponding to $q = 9.9e11$ W/m^3

that the size of the first element near the wall of the micro chamber should be equal to the dimension of the elements of the microfluidic device,

- To evaluate the different mesh size (see table 1 for more details about the mesh), the test process involved measuring the maximum velocity at each mesh size over different simulation time intervals, as shown in Figure 3. The results revealed a notable trend: beyond mesh size M4, the velocity of the bacteria-water mixture was remarkably insensitive to the mesh size used. This observation led to the decision to adopt the M4 mesh grid for the remainder of our simulations, as it struck a balance between accuracy and computational efficiency. The use of this specific grid was intended to guarantee the consistency and reliability of our simulation results.

- ANSYS fluent was used for numerical simulation,

- For pressure-velocity coupling, Fluent's built-in SIMPLE algorithms, were employed,

- Spatial discretization of the energy and momentum equations was achieved using Fluent's second-order scheme,

- Transient behaviour was accurately captured using Fluent's bounded second-order implicit scheme.

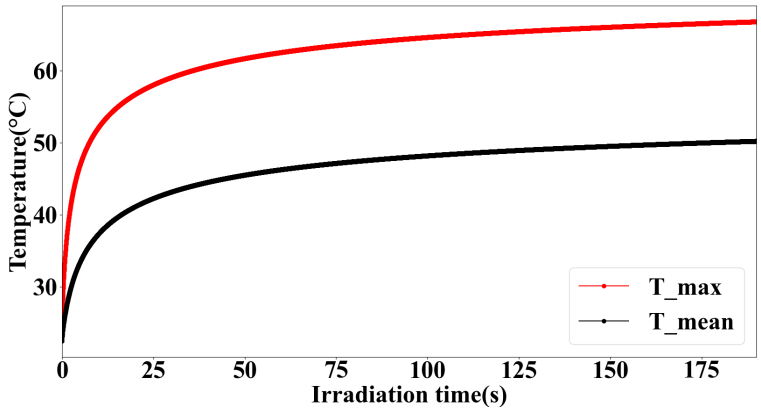

Fig. 7 Average and maximum temperature inside the fluidic chamber during the irradiation process for P=0.8 W corresponding to $q = 9.9e11$ W/m^3

4. RESULT

Figure 4 offers a comprehensive evaluation of our numerical simulations against experimental results. Figure 4 (a) represents a direct comparison with a benchmark case validates our numerical model's accuracy in capturing temperature dynamics in the microfluidic chamber. Figure 4 (b) provides a detailed comparison of temperature fields, emphasizing the agreement between theoretical predictions and experimental data at the borosilicate glass bottom. The temperature rise was predicted as a result of laser irradiation on the gold nanoparticles within the chamber (see Fig 5). The peak temperature reflects the maximum thermal effect achieved during the process. The temperature increase observed implies that thermal inactivation of bacteria is enhanced with higher laser power.

The temperature field results at different simulation times ($t = 10s$, $t = 40s$, $t = 120s$, $t = 190s$ irradiation time) reveal a dynamic evolution within the microfluidic chamber. As shown in the Figure 6, the diffusion pattern illustrates a remarkable trend: higher temperatures from the centre region progressively propagate towards the chamber boundary over time. At the initial time point ($t = 10s$), a concentrated temperature distribution is observed in the centre, indicating the immediate impact of laser irradiation. Then, at t=40s, the higher temperature zone extends radially outwards, indicating a continuous process of outward heat transfer. This trend continues at $t = 120s$ and $t = 190s$.In our observations, the diffusion pattern illustrates a progressive outward expansion of the region with higher temperatures. This means that, as the simulation progresses, the heat initially concentrated in the centre of the chamber disperses towards the periphery. The diffusion diagram demonstrates the effectiveness of the laser-induced thermal effects and the controlled heat transfer assisted by the gold nanoparticles. The temporal evolution of average and maximum temperatures inside the microfluidic chamber reveals a detailed scenario of thermal processes during laser irradiation (see Figure 7). Initially, there is a rapid increase in mean and maximum temperatures, observed up to around $25s$. This rapid escalation is a manifestation of the immediate impact of laser energy absorption by gold nanoparticles, leading to a localized zone of high temperature. Subsequently, beyond the initial phase, a transition takes place towards a slower, sustained increase in average and maximum temperatures. This change indicates the establishment of a dynamic equilibrium within the system. As the microfluidic chamber absorbs the initial energy, a balance is found between continuous laser irradiation and heat dissipation. This observed trend, particularly with regard to average and maximum temperatures, summarizes the nuanced processes governing temperature evolution during laser bacterial inactivation. The initial rapid rise highlights the immediate response to energy input, while the subsequent slower increase underlines the establishment of a thermal equilibrium as the system adapts to continuous laser irradiation.

Temporal profiles of bacterial concentration, combined with contours showing bacterial concentration at the bottom of the chamber, provide a dynamic representation of bacterial response to laser irradiation over time

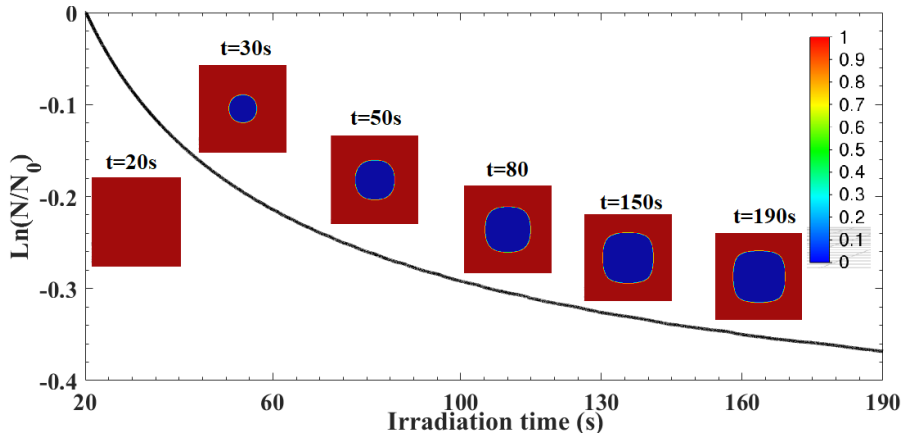

Fig. 8 Temporal profiles of bacterial concentration in the entire chamber for P=0.8 W corresponding to $q = 9.9e11$ W/m^3 . The sub-figure highlights the contours of bacterial concentration on chamber bottom: from a high concentration (red) to zero (blue)

(see Figure 8). On the x-axis representing time and the y-axis representing $Ln(N/N_0)$, the natural logarithm of the ratio of the current bacterial concentration (N) to the initial concentration (N_0), a perceptible reduction in bacterial concentration develops. Values of $Ln(N/N_0)$, starting from 0 and gradually falling below 0, indicate a decrease in the bacterial population. This indicates the progressive inactivation of bacteria in response to the increased temperatures caused by laser irradiation. Remarkably, the contours of the chamber bottom reveal a spatial aspect of the dynamics of bacterial concentration. At $t = 30s$, a pivotal point is observed where bacterial concentration begins to decrease from the central region, indicating the onset of bacterial inactivation. This central region acts as a focal point for the onset of bacterial inactivation, and as time passes, this zone expands outwards. The contours, ranging from high concentration (red) to zero (blue), clearly illustrate the spatial distribution of inactivated bacteria, underlining the effectiveness of laser-induced bacterial control. The initiation of inactivation in the central region suggests a localized response to laser energy, and as this response spreads, it leads to a progressive reduction in bacterial concentration.

5. CONCLUSION

This investigation employed CFD technique to model the inactivation of *E. coli* bacteria in a microfluidic chamber subjected to laser-irradiated gold nanoparticles. The adoption of a single-phase model, with effective thermal properties determined by established correlations, facilitated the incorporation of bacteria presence into the governing equations. The developed User Defined Function successfully implemented a first-order kinetic model guided by the Arrhenius equation, capturing the reduction in bacterial concentration over time. Our findings highlight the temporal and spatial dynamics of bacterial inactivation, emphasizing the crucial role of laser-induced thermal effects. This work advances our understanding of the intricate relationships between laser irradiation, gold nanoparticles, and bacterial response, laying the foundation for optimized laser-based bacterial control strategies across diverse applications, from healthcare to biotechnology.

ACKNOWLEDGMENTS

The work was supported by the National Science Centre, Poland, under research project “Shape and displacement optimization of gold nanorods in the killing chamber in order to photothermoablation processes”, no UMO-2021/43/D/ST8/02504. Computations were carried out using the computers of Centre of Informatics Tricity Academic Supercomputer & Network (CI TASK).

REFERENCES

[1] Vuerich, R., Martinelli, V., Vodret, S., Bertani, I., Carletti, T., Zentilin, L., Venturi, V., Marcello, A. and Zacchigna, S., 2022. A new laser device for ultra-rapid and sustainable aerosol sterilization. *Environment International*, 164, p.107272.

[2] Handorf, O., Pauker, V.I., Schnabel, U., Weihe, T., Freund, E., Bekeschus, S., Riedel, K. and Ehlbeck, J., 2020. Characterization of antimicrobial effects of plasma-treated water (PTW) produced by microwave-induced plasma (MidiPLexc) on Pseudomonas fluorescens biofilms. *Applied Sciences*, 10(9), p.3118.

[3] Chavan, P., Yadav, R., Sharma, P. and Jaiswal, A.K., 2023. Laser Light as an Emerging Method for Sustainable Food Processing, Packaging, and Testing. *Foods*, 12(16), p.2983.

[4] Liu, Y., 2018. Electrostatic precipitation of fine airborne particles and biological decontamination, efficiency and energy consumption tendencies. PhD thesis, University of Strathclyde

[5] Dheyab, M.A., Aziz, A.A., Khaniabadi, P.M., Jameel, M.S., Oladzadabbasabadi, N., Rahman, A.A., Braim, F.S. and Mehrdel, B., 2023. Gold nanoparticles-based photothermal therapy for breast cancer. *Photodiagnosis and photodynamic therapy*, p.103312.

[6] Tebele, M.F., Paris, G. and Zelcer, A., 2023. Plasmonic inhibition of bacterial adhesion on gold-decorated mesoporous zirconium oxide thin films. Colloids and Surfaces B: *Biointerfaces*, 232, p.113576.

[7] Abo-Neima, S.E., 2023. Biological Activity of Photodynamic Laser Radiation and Nickel Nanoparticles on Staphylococcus aureus Bacteria. *BioNanoScience*, 13(2), pp.704-717.

[8] Koulali, A., Ziółkowski, P., Radomski, P., De Sio, L., Zieliński, J. and Mikielewicz, D., Single-phase CFD approach for investigating bacterial inactivation and heat transfer in a microchamber. *XXV Jubileuszowy Zjazd Termodynamików*, p.167-170.

[9] Federica Zaccagnini, Piotr Radomski, Maria Laura Sforza, Pawel Ziółkowski, Seok-In Lim, KwangUn Jeong, Dariusz Mikielewicz, Nicholas P. Godman, Dean R. Evans, Jonathan E. Slagle, Michael E. McConney, Daniela De Biase, Francesca Petronella and Luciano De Sio , 2023. White light thermoplasmonic activated gold nanorod arrays enable the photo-thermal disinfection of medical tools from bacterial contamination. *Journal of Materials Chemistry B*, 11(29), pp.6823-6836.

[10] Giannelli, M., Pini, A., Formigli, L. and Bani, D., 2011. Comparative in vitro study among the effects of different laser and LED irradiation protocols and conventional chlorhexidine treatment for deactivation of bacterial lipopolysaccharide adherent to titanium surface. *Photomedicine and laser surgery*, 29(8), pp.573-580.

[11] Ahmed, E., El-Gendy, A.O., Moniem Radi, N.A. and Mohamed, T., 2021. The bactericidal efficacy of femtosecond laser-based therapy on the most common infectious bacterial pathogens in chronic wounds: An in vitro study. *Lasers in Medical Science*, 36, pp.641-647.

[12] Malenfant, D.J., Gillies, D.J. and Rehse, S.J., 2016. Bacterial suspensions deposited on microbiological filter material for rapid laser-induced breakdown spectroscopy identification. *Applied Spectroscopy*, 70(3), pp.485-493.

[13] Ziółkowski, P. and Badur, J., 2018. A theoretical, numerical and experimental verification of the Reynolds thermal transpiration law. *International Journal of Numerical Methods for Heat & Fluid Flow*, 28(1), pp.64-80.

[14] Angeloudis, A., Stoesser, T. and Falconer, R.A., 2014. Predicting the disinfection efficiency range in chlorine contact tanks through a CFD-based approach. *Water Research*, 60, pp.118-129.

[15] Zhang, J., Tejada-Martínez, A.E. and Zhang, Q., 2014. Developments in computational fluid dynamics-based modeling for disinfection technologies over the last two decades: A review. *Environmental modelling & software*, 58, pp.71-85.

[16] Jenny, R.M., Simmons III, O.D., Shatalov, M. and Ducoste, J.J., 2014. Modeling a continuous flow ultraviolet Light Emitting Diode reactor using computational fluid dynamics. *Chemical Engineering Science*, 116, pp.524-535.

[17] Feurhuber, M., Cattide, A., Magno, M., Miranda, M., Prieler, R. and Hochenauer, C., 2017. Prediction of the fluid flow, heat transfer and inactivation of microorganism at medical devices in modern steam sterilizers using computational fluid dynamics. *Applied Thermal Engineering*, 127, pp.1391-1403.

[18] Feurhuber, M., Burian, P., Magno, M., Miranda, M. and Hochenauer, C., 2019. CFD simulation of the inactivation of Geobacillus stearothermophilus on dental handpieces. *International Journal of Heat and Mass Transfer*, 144, p.118649.

[19] Feurhuber, M., Neuschwander, R., Taupitz, T., Schwarz, V., Frank, C. and Hochenauer, C., 2021. A Computational Fluid Dynamics (CFD) model to simulate the inactivation of Geobacillus stearothermophilus spores in different moist heat sterilization environments. *Physics in Medicine*, 12, p.100039.

[20] Samstag, R.W., Ducoste, J.J., Griborio, A., Nopens, I., Batstone, D.J., Wicks, J.D., Saunders, S., Wicklein, E.A., Kenny, G. and Laurent, J., 2016. CFD for wastewater treatment: an overview. *Water Science and Technology*, 74(3), pp.549-563.

[21] Santoro, D., Crapulli, F., Raisee, M., Raspa, G. and Haas, C.N., 2015. Nondeterministic computational fluid dynamics modeling of Escherichia coli inactivation by peracetic acid in municipal wastewater contact tanks. *Environmental Science & Technology*, 49(12), pp.7265-7275.

[22] Fujikawa, H. and Itoh, T., 1998. Thermal inactivation analysis of mesophiles using the Arrhenius and z-value models. *Journal of food protection*, 61(7), pp.910-912.

[23] Ghani, A.A., Farid, M.M., Chen, X.D. and Richards, P., 1999. An investigation of deactivation of bacteria in a canned liquid

food during sterilization using computational fluid dynamics (CFD). *Journal of food engineering*, 42(4), pp.207-214.

[24] Abu-Farah, L. and Germann, N., 2022. Simulations of thermal phase changes and bacterial inactivation in a superheated steam dishwasher. *Physics of Fluids*, 34(8).

[25] Koulali, A., Abderrahmane, A., Jamshed, W., Hussain, S.M., Nisar, K.S., Abdel-Aty, A.H., Yahia, I.S. and Eid, M.R., 2021. Comparative study on effects of thermal gradient direction on heat exchange between a pure fluid and a nanofluid: Employing finite volume method. *Coatings*, 11(12), p.1481.

[26] Brinkman, H.C., 1952. The viscosity of concentrated suspensions and solutions. *The Journal of chemical physics*, 20(4), pp.571-571.

[27] Radomski, P., Ziółkowski, P., de Sio, L. and Mikielewicz, D., 2021. Computational fluid dynamics simulation of heat transfer from densely packed gold nanoparticles to isotropic media. *Archives of Thermodynamics*, pp.87-113.

[28] ANSYS Inc. (2021). ANSYS Fluent (v2021 R1) [Computer software]. ANSYS Inc.